Nanotextures of aragonite in stromatolites from the quasi-marine Satonda crater lake, Indonesia

KARIM BENZERARA[1]*, ANDERS MEIBOM[2], QUENTIN GAUTIER[1], JÓZEF KAŹMIERCZAK[3], JAROSŁAW STOLARSKI[3], NICOLAS MENGUY[1] & GORDON E. BROWN, JR[4,5]

[1]*Equipe Géobiosphère Actuelle et Primitive, IMPMC & IPGP, UMR 7590, CNRS, Universités Paris 6 et IPGP. 140, rue de Lourmel, 75015 Paris, France*

[2]*Muséum National d'Histoire Naturelle, Laboratoire de Minéralogie et Cosmochimie du Muséum (LMCM), UMR 7202, Paris, France*

[3]*Institute of Paleobiology, Polish Academy of Sciences, Twarda 51/55, 00818 Warsaw, Poland*

[4]*Surface & Aqueous Geochemistry Group, Department of Geological & Environmental Sciences, Stanford University, Stanford, CA 94305-2115, USA*

[5]*Stanford Synchrotron Radiation Lightsource, SLAC National Accelerator Laboratory, Menlo Park, CA 94025, USA*

**Corresponding author (e-mail: karim.benzerara@impmc.jussieu.fr)*

Abstract: Stromatolites have been extensively used as indicators of ancient life on Earth. Although much work has been done on modern stromatolites, the extent to which biological processes control their structure, and the respective contributions of biological and abiotic processes in their formation are, however, still poorly constrained. A better description of the mineralogical textures of these formations at the submicrometre scale may help improve our understanding of how carbonates nucleate and grow in stromatolites. Here, we used a combination of microscopy and microspectroscopy techniques to study the chemical composition and the texture of aragonite in lacustrine stromatolites from the alkaline crator lake in Satonda, Indonesia. Several textural features are described, including morphological variations of aragonite from nanosized grains to micrometre-sized fibres, the presence of striations in the aragonite laminae showing a striking similarity with growth bands in corals, and clusters of small aragonite crystals sharing a common crystallographic orientation. These nanotextural features are compared with those observed in scleractinian corals, and possible processes involved in their formation are discussed.

Stromatolites are laminated sedimentary growth structures, usually composed of calcium carbonates, with growth initiated from a point or a limited surface (Semikhatov *et al.* 1979). They have been found throughout the geological record as far back as 3.5 Ga ago (e.g. Hofmann 2000). As modern stromatolites are systematically and intimately associated with microbial communities, ancient stromatolites have often been considered to be one of the oldest traces of life on Earth (Hofmann 2000; Altermann *et al.* 2006; Schopf *et al.* 2007). The biogenicity of many ancient stromatolites has, however, been questioned in particular because very few microfossils have been found in these samples (e.g. Lowe 1994; Grotzinger & Rothman 1996; Lepot *et al.* 2008) and similar morphological patterns can be produced abiotically (Grotzinger & Rothman 1996; McLoughlin *et al.* 2008). The macroscopic morphology (e.g. Allwood *et al.* 2006) as well as the mesostructure (Shapiro 2000) of stromatolites are important tools presently used to infer the biogenicity of ancient stromatolites. New numerical models allowing exploration of the various possible morphologies of stromatolites and assessment of the respective roles of environmental and biological processes in their formation have been proposed by Dupraz *et al.* (2006). These authors note that a detailed mechanistic description of how stromatolites are formed is still warranted. Such a description may benefit from a more detailed characterization of the mineral and organic building units of stromatolites and their arrangement at the submicrometre-scale, that is, the scale at which nucleation and mineral growth take place. However, one difficulty is that this approach requires the use of specialized analytical tools, as the building units of

From: PEDLEY, H. M. & ROGERSON, M. (eds) *Tufas and Speleothems: Unravelling the Microbial and Physical Controls*. Geological Society, London, Special Publications, **336**, 211–224.
DOI: 10.1144/SP336.10 0305-8719/10/$15.00

carbonates can be very small (in the few tens of nanometre size range).

In the present study, we focus on the morphology and arrangement of carbonate crystals in recent subfossil (possibly several hundreds of years old) lacustrine stromatolites. The combination of microscopy and microspectroscopy tools such as scanning and transmission electron microscopy (SEM and TEM), NanoSIMS and synchrotron-based scanning transmission X-ray microscopy (STXM) provides unique information on the compositional variations and mineral textures or microfabrics of stromatolites at the submicrometre scale. Several textural features show a remarkable similarity to those observed in modern corals. These similarities as well as differences are discussed in light of the mineralization processes by which modern stromatolites and corals form. Although these results are of interest to the scientific community working on microbialites, the approach and the basic mineral building units that are described should be of general interest to communities working on carbonate precipitates such as tufas and speleothems.

Material and methods

Stromatolite samples

Modern subfossil stromatolite samples were collected from the crater lake of Satonda, a small volcanic island in Indonesia previously described in detail by Kempe & Kaźmierczak (1993, 2007), Arp *et al.* (2003) and Kazmierczak & Kempe (2004). We studied sample S-47, collected with from the stromatolitic reefs at station 10 above the water table (see Kempe & Kazmierczak, 1993). These stromatolites are actually subfossil and, although we do not know precisely their age, may be as old as several hundred years. Some features may have been modified by aging (e.g. some organic functions), but the transformation of mineral textures seems unlikely considering that: (1) the samples have remained at the surface; (2) they are still composed of aragonite and not calcite as would be expected from prolonged interaction with meteoric water; and (3) the same mineral textures are observed in other genuinely modern microbialites from alkaline lakes (e.g. from Lake Van in Turkey). As a comparison, the earliest steps of diagenesis of aragonite structures, which can be observed after a few years, have been studied for example by Perrin & Smith (2007). Satonda Lake is a slightly alkaline (pH 8.55) quasi-seawater system that harbors calcareous stromatolites along the shore. The laminations of Satonda stromatolites consist of alternating 50–500 μm thick aragonite laminae and 1 to a few tens of micrometres thin Mg–Si-containing layers. Some fragments of the Satonda stromatolites were powdered for XRD and TEM analyses to characterize the nature and morphology of the crystals comprising them. In order to spatially resolve textural and chemical information within the structure of Satonda stromatolites, petrographic thin sections were prepared and gold-coated for SEM and NanoSIMS analyses. Some spots were selected for preparation of ultrathin electron-transparent foils (less than 100 nm in thickness) by Focused Ion Beam milling. These foils were further analysed at the few nanometer spatial scale by scanning transmission X-ray microscopy (STXM) and TEM.

Scanning electron microscopy

SEM analyses were performed on the Zeiss Supra 55 SEM microscope in the Laboratory Magie at University Pierre et Marie Curie (Paris, France). The microscope was operated at 10 kV with a working distance of 3 mm. Two different detectors were used: an in-Lens detector for secondary electron imaging (nano-topography of the sample) and an Angle selective Backscattered (AsB) detector for low-angle backscattered electrons which provide a contrast more sensitive to crystal orientation.

Following NanoSIMS analyses, the gold coating was removed from the petrographic sections and the samples were etched using a slightly acidic solution consisting of formic acid diluted to 0.1% in de-ionized milliQ water with 2% glutaraldehyde. The samples were re-coated with gold-palladium and observed by SEM.

Focused ion beam milling

Focused ion beam (FIB) milling was performed with a FEI Model 200 TEM FIB system at the University Aix-Marseille III. The FIB lift-out method was used to prepare a cross-section across one Mg–Si-rich area surrounded by two aragonite laminae. This method is described in detail in Heaney *et al.* (2001) and Benzerara *et al.* (2005). A thin strip of platinum was deposited on the area of interest in order to protect it during the milling process. A 30 kV Ga+ beam operating at *c.* 20 nA excavated the sample from both sides of the Pt strip to a depth of 5 μm. Before removal of the thin foil, it was further thinned to *c.* 100 nm with a glancing angle beam at much lower beam currents of *c.* 100 pA. Finally, a line pattern was drawn with the ion beam along the side and bottom edges of the thin foil allowing its removal from the sample. The slide was transferred at room pressure with a micromanipulator onto the membrane of a formvar-coated 200 mesh copper grid for TEM and STXM analyses.

Transmission electron microscopy

Two types of samples were used for TEM work: (1) powders that were suspended for a few seconds in distilled water then deposited on the membrane of a lacey carbon-coated 200 mesh copper grid and air dried; and (2) the FIB ultrathin foil. TEM observations were carried out at IMPMC on a JEOL 2100F microscope operating at 200 kV, equipped with a field emission gun and a high resolution UHR pole piece. A double-tilt sample holder was used to orient samples during the collection of TEM images and electron diffraction patterns from the samples.

Scanning transmission X-ray microscopy (STXM)

STXM is a type of transmission microscopy that uses a monochromated X-ray beam produced by synchrotron radiation. The rationale for STXM data acquisition and analysis and examples of applications can be found in Hitchcock (2001) and Bluhm *et al.* (2006). For STXM imaging, the X-ray beam is focused on an X-ray transparent sample using a zone plate, and a 2-D image is collected by scanning the sample at a fixed photon energy. The achieved spatial resolution is dependent on the zone plate and was *c*. 25 nm in the present study. The image contrast results from differential absorption of X-rays, which partly depends on the chemical composition of the sample. In addition to imaging, it is possible to perform at the same spatial resolution, near edge X-ray absorption fine structure (NEXAFS) spectroscopy at the carbon K-edge (or other absorption edges in the 80–2000 eV energy range) which gives information on the speciation (i.e. type of functional group and bonding) of carbon (or other elements). In this present case, it was thus possible to detect an absorption feature at 290.3 eV corresponding to $1s \rightarrow \pi^*$ electronic transitions in the carbonate group. It has been shown previously that the absorption intensity at 290.3 eV depends on the orientation of the aragonite *c*-axis (i.e. the direction of the carbonate π^* orbitals) relative to the polarization of the synchrotron X-ray beam (e.g. Metzler *et al.* 2008). This phenomenon is known as linear dichroism. The absorption at 290.3 eV is maximum when the *c*-axis of aragonite parallels the polarization vector of the beam and minimum when they are perpendicular (see Fig. 6). At 290.3 eV, we acquired ten different images of the FIB foil, each at a different polarization of the synchrotron X-ray beam ranging from horizontal (noted as 0°) to vertical (noted as 90°). These images were converted to a linear absorbance (optical density, OD) scale

$$OD = \ln(I/I_0) \quad (1)$$

where I is the transmitted intensity and I_0 is the incident beam measured in a region adjacent to the foil that contains no sample. The resulting images were aligned carefully. The carbonate OD of each individual pixel was then fit using a routine written with the statistical software R as a function of the polarization angle using the following equation:

$$OD(\alpha) = C + A^* \cos^2(\alpha - \phi) \quad (2)$$

where α is the polarization of the incident X-ray beam (from 0 to 90°), ϕ is the angular orientation of the *c*-axis of aragonite (from 0 to 180°), C is the in-plane polarization-independent fraction of the absorption, and A is the amplitude of the polarization-dependent absorption. From these measurements the crystallographic orientation of the *c*-axis (ϕ) of aragonite was plotted for each individual pixel (here, at the 50-nm scale) on the whole FIB foil providing the map reported in Figure 6.

STXM observations were performed at the Advanced Light Source (ALS) (Lawrence Berkeley National Laboratory) on MES branch line 11.0.2.2. During our measurements, the ALS storage ring operated at 1.9 GeV and 200–400 mA stored current. A 1200 l/mm grating and 40 μm exit slits in both dispersive and non-dispersive direction were used for carbon imaging and spectroscopy, providing a theoretical energy resolution of 72 meV. Energy calibration was accomplished using the well-resolved 3p Rydberg peak at 294.96 eV of gaseous CO_2 for the C K-edge.

NanoSIMS

Spatially resolved determination of Mg/Ca and Sr/Ca ratios along profiles within the carbonate laminae of the Satonda stromatolites was carried out using the Cameca NanoSIMS N50 at the Muséum National d'Histoire Naturelle in Paris with the same settings as in Meibom *et al.* (2007, 2008). Using a primary beam of O^-, secondary ions of $^{24}Mg^+$, $^{40}Ca^+$, and $^{88}Sr^+$ were sputtered from the sample surface and detected simultaneously in electron multipliers at a mass resolving power of *c*. 4000. At this mass-resolution all potentially problematic interferences are resolved. The data were obtained from a pre-sputtered surface in a series of line-scans with the primary ions focused to a spot-size of *c*. 150 nm. Magnesium and Sr concentrations were calibrated against carbonate standards of known composition.

Results

The modern subfossil stromatolites from Satonda that have been analyzed in the present study consist of aggregated mm-sized laminated circular

overgrowths on filamentous green algae thalli (Fig. 1). These samples show a facies that was named 'stromatolitic-siphonocladalean' and 'peloidal zone' by Kempe & Kaźmierczak (1993) and 'Green-Algal Microbialite' by Arp *et al.* (2003). This facies comprises a significant part of the Satonda reef framework the bulk of which is composed of marine stenohaline calcareous red algae

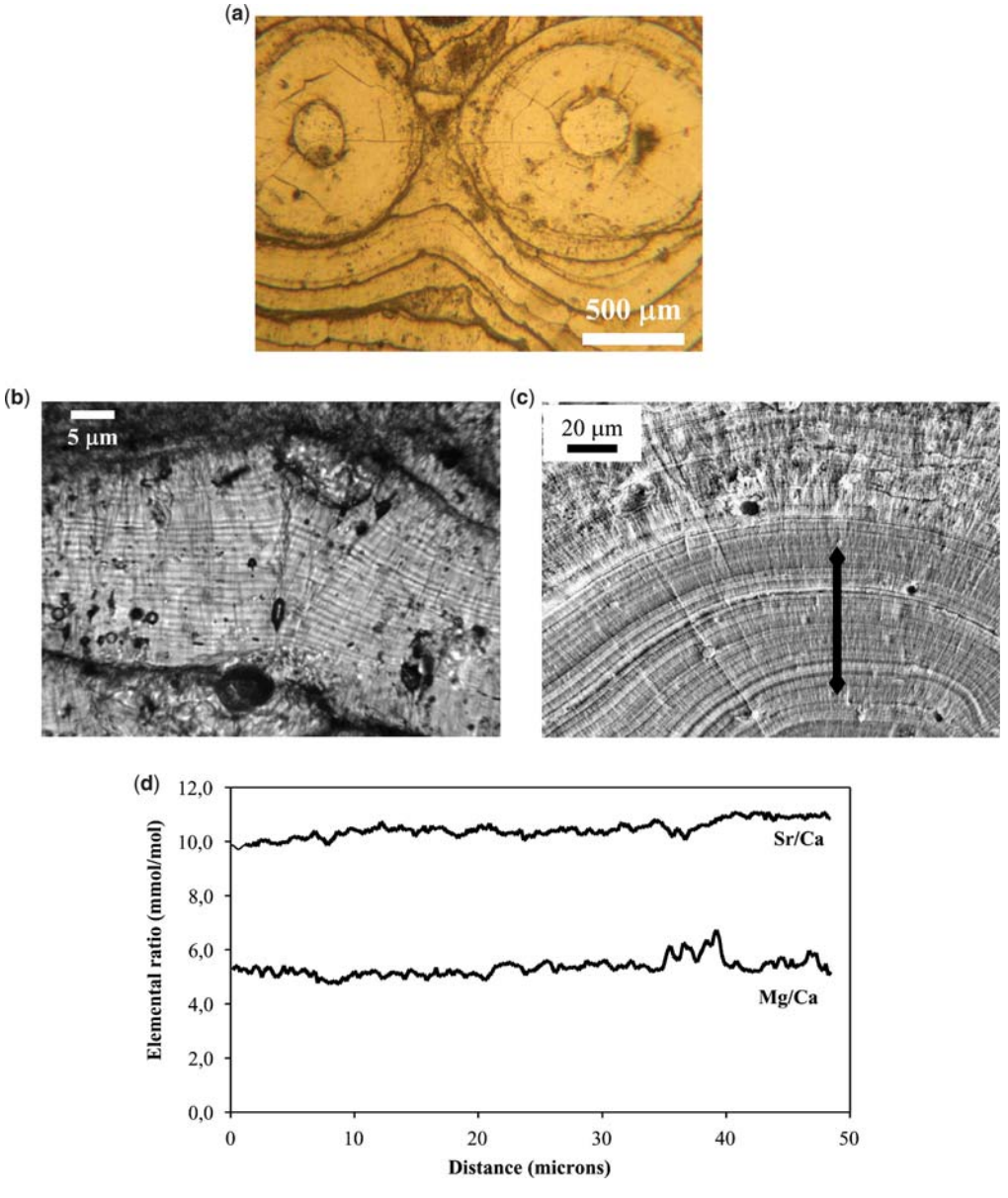

Fig. 1. Observation and compositional analysis of carbonate laminae in Satonda stromatolites. (**a**) Optical microscopy image of the laminated circular overgrowths on filamentous green algae forming the framework of Satonda stromatolites. Concentric dark (Mg–Si rich) and bright (aragonite) laminae can be observed. (**b**) Optical microscopy image of one aragonite lamina at higher magnification showing striations parallel to the general direction of the lamina accretion. The average distance between striations is around 1 μm. (**c**) Secondary electron SEM image of the laminae which have been slightly etched. The fibrous texture of the aragonite laminae as well as numerous striations are visible. (**d**) NanoSIMS measurements of the Sr/Ca and Mg/Ca ratios along a 50-μm segment profile.

(*Peyssonnelia* and *Lithoporella*) and nubecullinid foraminifers. The laminated overgrowths show alternation of a poorly crystallized Mg–Si-rich mineral phase (thin and dark in transmitted light optical microscopy) described by Arp *et al.* (2003) and aragonite, forming thick and bright laminae in transmitted light optical microscopy. We focused on the aragonite laminae for the textural analyses. A detailed description of the texture of aragonite laminae might help to better understand the potential role of microorganisms in their formation.

Aragonite laminae can be as thick as a millimetre and most of them show fine striations in transmitted light microscopy parallel to the accretion planes of the laminae (Fig. 1). This striated texture could also be observed by SEM on samples etched gently with formic acid. These striations were also described by Kempe & Kaźmierczak (1993), but their origin remains mysterious. Interestingly, these striations show a striking similarity with the growth bands observed in the fibrous aragonite skeleton of scleractinian corals (Fig. 2, e.g. Meibom *et al.* 2004). As these bands correlate with significant Mg and Sr variations in corals, we measured the same elemental profiles within the aragonite laminations by NanoSIMS (Fig. 1). In contrast to what has been observed for corals (e.g. Meibom *et al.* 2007, 2008), no significant variations of the Sr/Ca ratio were observed in the aragonite laminae. The slight increase of Mg/Ca at 36 microns was very small compared to what is usually observed in corals and moreover, this ratio was constant for the rest of the profile and did not show systematic variations within the striations observed by SEM.

TEM observations on powdered samples of the crystal units forming the Satonda stromatolites showed only a poorly crystallized Mg–Si-rich phase and aragonite, consistent with bulk XRD measurements. Although powdering destroys the textural relationship between crystals, these observations were nonetheless useful because they showed that the aragonite can have two different morphologies (Fig. 3): (1) some aragonite appears as single-crystal fibres that are a few micrometres in length and a few hundred nanometres in width; and (2) the remainder of the aragonite appears as small globules a few tens of nanometres in size and forms polycrystalline clusters. This latter texture is usually called micritic and has been observed by many authors in the past (e.g. Riding 2000; Dupraz *et al.* 2004).

To obtain more information on the spatial distribution of these types of morphologies in the aragonite laminae of Satonda stromatolites, non-etched petrographic thin sections were examined by SEM. As previously reported by Kempe & Kaźmierczak (1993) and Arp *et al.* (2003), the aragonite laminations appear at first sight to be mostly fibrous, with aragonite fibres perpendicular to the laminae surface (Fig. 4). However, at higher magnification, these fibres seem to consist of clusters of nanocrystals that are similar in size to the nanocrystals found in the powdered samples. SEM observations of such tiny domains may however be misleading as they probe the very near surface of the sample which might be very sensitive to the sample preparation protocol, to slight etching during the polishing stage and/or to artifactual nanograins that may have formed during the gold-palladium coating procedure (Gibbs & Powell 1996; Steele *et al.* 1998). The use of other techniques that require minimal sample preparation such as cryo-SEM and/or environmental SEM would be a useful approach to better address this issue (e.g. Dupraz *et al.* 2004). Another approach consists of preparing the samples for techniques that are not surface-sensitive such as TEM or STXM.

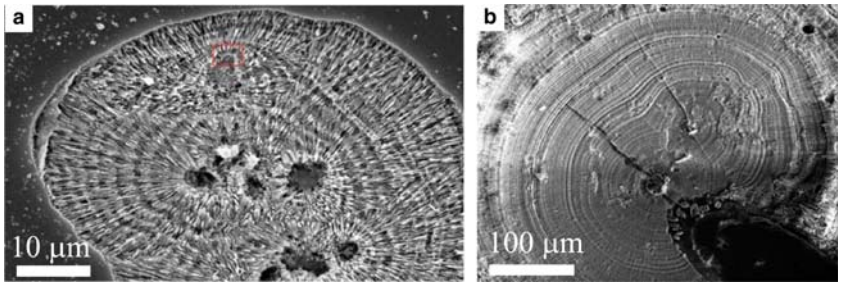

Fig. 2. Comparative SEM images of *Porites sp.* skeleton (**a**) and Satonda stromatolites (**b**). Both samples were gently etched with formic acid (1%). (a) Centres of rapid accretion can be observed as pits in the centre of the image. Concentric growth bands as well as aragonite fibres are visible on this etched sample. (b) Two pits can be observed at the center of the structure. They have classically been interpreted as remnants of green algae around which the carbonates precipitate. Concentric growth bands can be observed. Aragonite fibres can be observed at higher magnification (see Fig. 4).

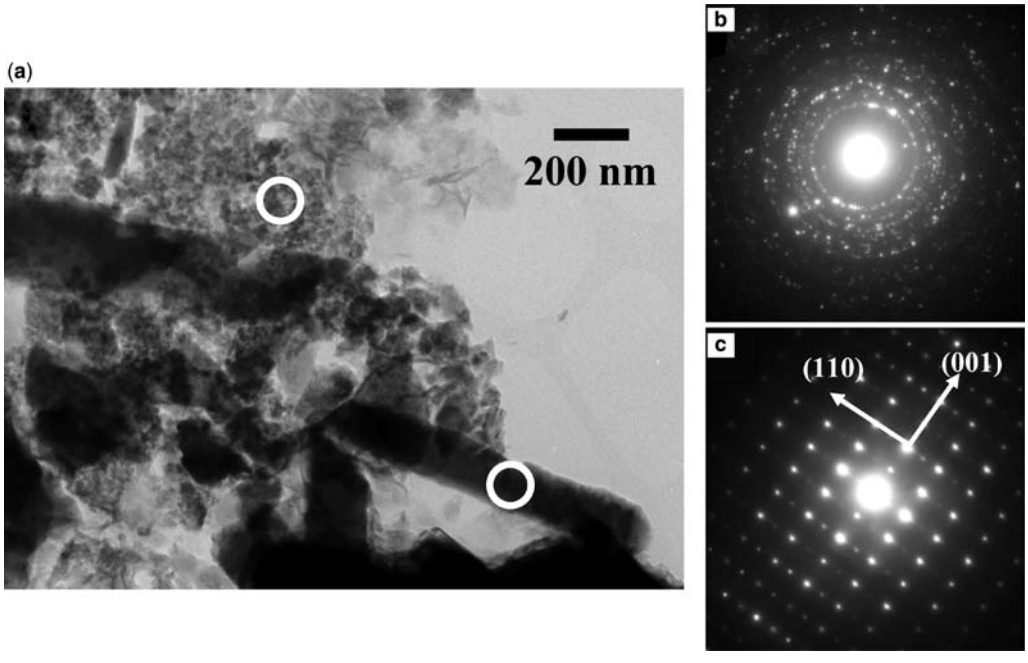

Fig. 3. TEM observation of powders of the Satonda stromatolites. (**a**) Bright field image showing aragonite fibres as well as clusters of very small aragonite grains. The circles indicate the locations where electron diffraction patters were measured (upper one on the cluster, lower one on a fibre). (**b**) The powder pattern shows spacings at 4.2, 3.4, 2.9, 2.7 and 2.5 Å, which can be indexed as due to diffraction from the (110), (111), (002), (121) and (200) planes of aragonite. (**c**) The single crystal diffraction pattern is consistent with aragonite and was measured along the [1–10] zone axis.

We investigated the crystallographic orientation of the aragonite in more detail by TEM and STXM using a FIB-milled ultrathin foil, which was cut across a Mg–Si-rich layer (Fig. 5). On both sides of this layer, we observed the top of the underlying aragonite laminae (left in Fig. 5) and the bottom of the overlying aragonite laminae (right in Fig. 5). The two distinct morphologies of aragonite observed in the powdered samples were also observed in this foil. In the top part of the underlying aragonite laminae, aragonite appears as bundles of single-crystal fibres, with their growth axes parallel to each other and perpendicular to the laminae. In contrast, aragonite in the overlying aragonite laminae appears as a massive cluster of tiny aragonite crystals (*c*. 50 nm in size). The orientation of the aragonite crystals in the FIB foil can be assessed by electron diffraction. Single-crystal electron diffraction patterns were obtained using a 100-nm large aperture on the fibre area. These patterns show unambiguously that aragonite fibres share a common crystallographic orientation (Fig. 5). Powder electron diffraction patterns were obtained on the clusters of tiny aragonite crystals using a 1-μm large aperture. The clustering of some spots on some rings suggests some orientation of the nanocrystals. It is difficult, however, to get a more comprehensive view of the crystallographic orientation of aragonite in the foil. To obtain a more complete view of the crystallographic orientation of these very small aragonite domains, we thus carried out STXM imaging and polarization-dependent imaging contrast on the entire FIB-milled foil. STXM has classically been used in the Earth Sciences to characterize the speciation of diverse elements such as C, N, O and heavy metals and metalloids such as at the nanoscale (e.g. Haberstroh *et al.* 2006; Bernard *et al.* 2007; Benzerara *et al.* 2008; Lepot *et al.* 2008). Some organic carbon could be detected by STXM in the FIB foil (data not shown); however, it was not possible to decipher whether this organic carbon was indigenous or was an artifact resulting from impregnation of the sample with epoxy. Here, we used the sensitivity of X-ray absorption spectroscopy to the crystallographic orientation of aragonite, an effect commonly referred to as X-ray linear dichroism (e.g. Metzler *et al.* 2008; Zhou *et al.* 2008). By varying the direction of the polarization vector of the X-ray beam from 0 to 90° in 10° steps and measuring the absorption of X-rays at 290.3 eV for each 50-nm pixel of the FIB-milled foil, it was possible

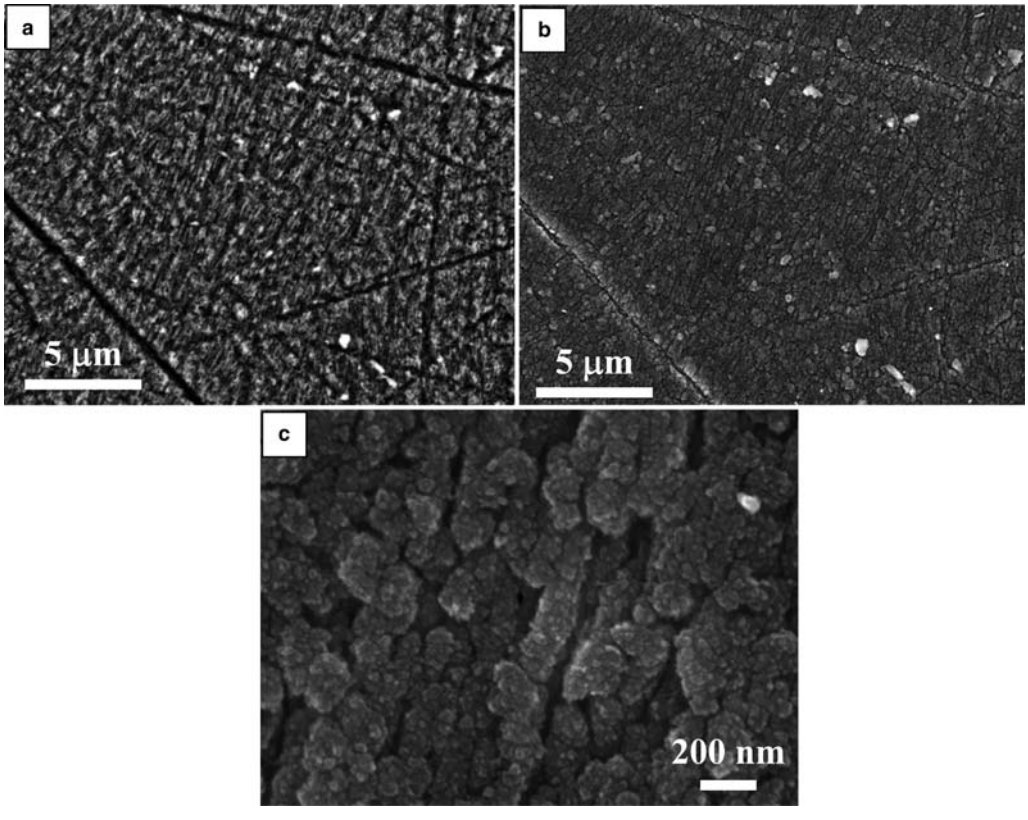

Fig. 4. SEM observation of polished sections of the Satonda stromatolites. (**a**) Image of an aragonite lamina collected in the low angle backscattered electron mode and revealing crystal directions. The fibrous texture is visible and the aragonite crystals are mostly oriented NNE–SSW. (**b**) Image of the same area collected in the secondary electron mode and showing the aragonite fibres. (**c**) At higher magnification, these fibres show a rough surface and seem to consist of an aggregation of tiny crystals.

to map the orientation of the in-plane projection of the *c*-axis of aragonite (Fig. 6). Interestingly, although TEM provides a better spatial resolution for imaging than STXM, it is limited for electron diffraction by the size of the smallest aperture, that is, in this case, 100 nm. This is larger than the spatial resolution achieved by STXM for the mapping of the orientation of aragonite *c*-axis as shown hereafter. Finally, STXM polarization-dependent imaging contrast is much less sensitive to variations of the orientation of aragonite than electron diffraction, in particular out-of-plane variations, and can thus be more efficient in providing an average view of the crystallographic texture of aragonite in the whole FIB foil. From this dataset, several observations can be made. First, the aragonite laminae are composed of micrometre-sized domains that respond homogeneously to the polarization changes (see areas 1, 2, 3 and 4 in Fig. 6). This response means that the in-plane projections of the *c*-axes of the grains present within these areas share a common orientation. Area 4 corresponds to the bundle of aragonite fibres observed by TEM in the aragonite laminae underlying the Mg–Si-rich laminae. The whole area is more absorbing at 0° than at 90°. The fit of the variation of absorption in $A \cos^2(\theta - \phi)$ gives a single value for the orientation of the *c*-axis of aragonite (ϕ) which is around 155° (equivalent to −25°). The STXM data thus confirm that the *c*-axes of these crystals (which are also the growth axes of aragonite) are roughly parallel to each other and parallel to the growth axis of the fibres as observed by TEM. Area 3 corresponds to the massive cluster of nanocrystals observed in Figure 5 at the bottom of the underlying aragonite layer. Interestingly, this area also shows a homogeneous response to the variations of polarization direction, with a ϕ value of 107°. This observation suggests that the *c*-axes of these nanocrystals also show a preferential orientation. It is

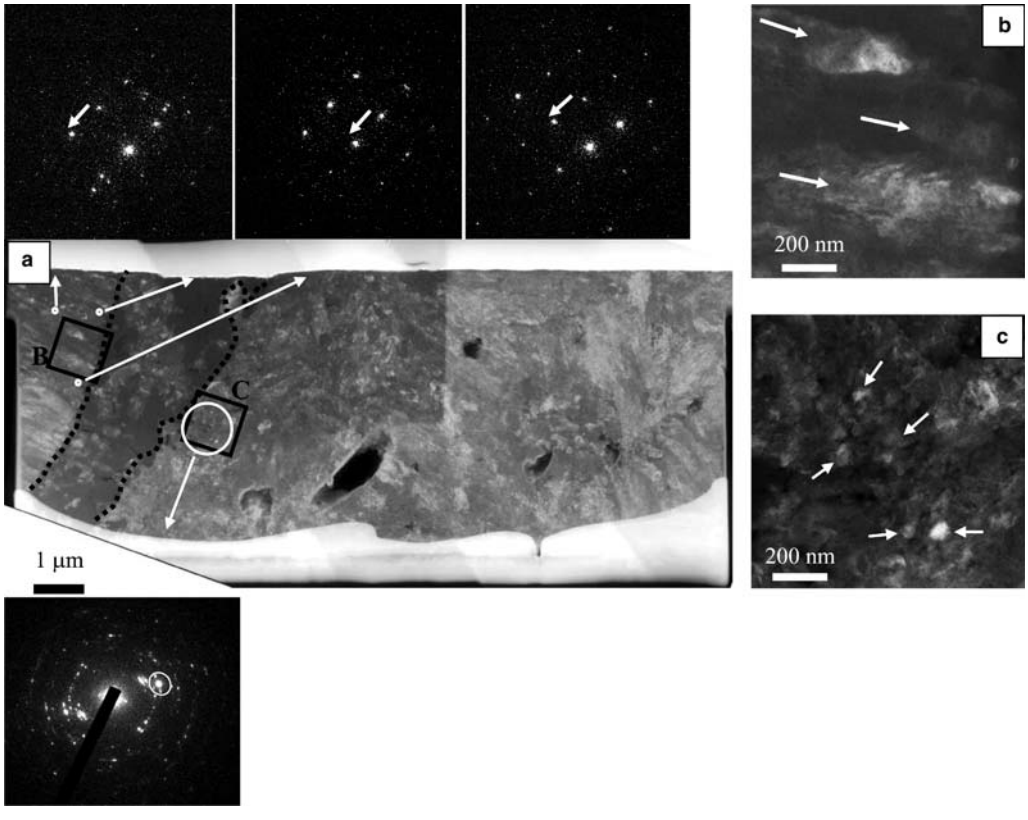

Fig. 5. TEM imaging of the FIB foil. (**a**) Negative image (bright field mode) of the whole FIB foil. The Si–Mg-rich lamina appears as a smooth dark grey area on the left hand side of the foil (area delimited by the dashed curves). Three electron diffraction patterns were obtained from different areas in the fibre area with a 100-nm wide aperture showing a common crystallographic orientation. One electron diffraction pattern was measured on the right hand side of the Mg–Si-rich lamina using a 1-μm wide aperture. On this powder pattern, the clustering of diffraction spots shows a common crystallographic orientation of different grains within the probed area. On the left hand side of the Mg–Si-rich lamina aragonite appears as fibres (see magnified image). (**b**) Arrows indicate the general direction of the fibres. On the right hand side, aragonite appears as clustered small domains [some grains are indicated by arrows in the magnified image (**c**)].

possible that these nanocrystals form larger-scale fibres by clustering, as supported by SEM images, but this cannot be ascertained based on TEM and the STXM images. STXM offers, however, a view differing from that of SEM. While SEM images show a general fibrous texture within the carbonate laminae with fibres perpendicular on average to the laminae surfaces, STXM suggests that the orientation of the in-plane projection of the *c*-axis of aragonite varies significantly within a lamina from the bottom to the top.

Discussion

The present study provides a basic description at the submicrometre-scale of the mineral texture of aragonite in Satonda stromatolites. Some textural features have been previously observed using more classical methods and include the heterogeneous microfabrics with either micritic (fine-grained) or sparitic (fibres) textures (e.g. Riding 2000) that have been related to various biotic or abiotic mineralization processes. Yet, some of these features are interesting in the light of their formation mechanism. Stromatolites have often been considered as biologically induced formations, that is, resulting from chemical variations (e.g. pH, alkalinity) indirectly induced by the metabolic activity of diverse microorganisms such as cyanobacteria and/or sulphate-reducing bacteria (e.g. Dupraz & Visscher 2005; Altermann *et al.* 2006). In addition to these metabolic processes, it has been shown that extracellular polymeric substances (EPS) may play a complex but significant role in the

precipitation of calcium carbonates (e.g. Braissant *et al.* 2007). In contrast, coral skeletons are usually considered as biologically controlled deposits, with specific genes controlling the achievement of the coral architecture, although a significant phenotypic plasticity due to environmental conditions is also observed (Todd 2008). The main conclusions of this general view are not contested here. There are obvious structural differences between corals and stromatolites such as the absence of centers of rapid accretion (i.e. centres of calcification) in stromatolites, variations in the orientation of the *c*-axes of aragonite within a single stromatolite lamina that are not visible in corals, or the absence of Mg–Si-rich laminae in corals. However, in the present study we show that some textural features, which have been attributed specifically to corals in the past and interpreted as the result of a biologically controlled process (e.g. clusters of nanocrystals within the centres of rapid accretion, crystallographic alignment of aragonite crystals, striations interpreted as growth bands), can also be found in stromatolites.

Two alternative conclusions can be drawn from this comparison: (1) biologically controlled mineralization processes may also play a role in the formation of Satonda stromatolites, at least to a certain extent; or (2) these textural features for which the precise mode of formation is unknown cannot be used as signatures of bio-controlled processes in corals. Using a reductionist but possibly heuristic approach, we discuss below some of the similarities and differences in the mineralogical textures of corals v. stromatolites at the submicrometre-scale.

From a mineralogical point of view, it is interesting to note that corals are assemblages of basic units consisting of aragonite fibres, aragonite nanoglobules (forming centres of calcification in scleractinian corals), and organic polymers (associated with the fibres as well as centers of rapid accretion, e.g. Stolarski 2003; Cuif & Dauphin 2005). No centre of rapid accretion (i.e. micrometre-sized clusters of aragonite nanocrystals with a very precise crystallographic alignment), was observed in Satonda stromatolites. However, Satonda stromatolites show similar fibrous, single-crystal aragonite as well as aragonite nanocrystals. Moreover, several studies have previously shown that aragonite or calcite nanocrystals are often associated with organic polymers in stromatolites (e.g. Kawaguchi & Decho 2002; Kühl *et al.* 2003; Kazmierczak *et al.* 2004; Dupraz & Visscher 2005; Benzerara *et al.* 2006; Kremer *et al.* 2008). The reason why two types of aragonite morphologies (fibrous v. micritic) are observed in these objects is not clear. Several authors have proposed for Satonda stromatolites as well as for corals that the micritic texture in both coral and stromatolites may be the result of precipitation in organic-enriched microenvironments (centers of rapid accretion in corals, or in living or partially degraded biofilms in stromatolites), while fibres would form in an organic-poor environment (e.g. Kempe & Kaźmierczak 1993; Arp *et al.* 2003; Stolarski 2003; Kempe & Kaźmierczak 2007). This proposal is supported by observations that aragonite nanocrystals within microbialites are surrounded by organic polymers (e.g. Benzerara *et al.* 2006) and that the experimental precipitation of carbonates in an organic matrix results in the formation of numerous and very small grains (Sethmann *et al.* 2005; Aloisi *et al.* 2006). In stromatolites from the Bahamas, three different types of microbial communities exhibiting different physical structures were identified. Micritic laminae composed of small aragonite fibres and not nanospheroids were shown to be specific to one of these communities (Reid *et al.* 2000; Visscher *et al.* 2000; Petrisor *et al.* 2004). It should be noted that in these open marine stromatolites, aragonite fibres can nucleate within EPS-rich biofilms, balancing the idea that fibres would always be associated with organic-deprived environments (Reid *et al.* 2000; Visscher *et al.* 2000). Finally, it has been shown that different EPS have various affinities for cations and may produce various polymorphs of calcium carbonate (e.g. Braissant *et al.* 2003), suggesting an additional source of variety in the texture of calcium carbonates.

There are genuine single-crystal aragonite fibres within stromatolites as observed in the present study (e.g. Fig. 3). They share a preferential crystallographic orientation along the growth axis (*c*-axis), perpendicular to the laminae, suggesting an abiotic growth process that initiates from an underlying surface. In contrast, some fibres may have formed by the clustering of aragonite nanocrystals resulting in what have been called mesocrystals, when nanodomains share a common crystallographic orientation. The existence of such mesocrystals in stromatolites is suggested by the STXM polarization-dependent images in the present study. Their presence in microbialites may have been overlooked in the past and will have to be assessed more thoroughly in the future. Interestingly, the aggregation of oriented vaterite nanocrystals with *c*-axis normal to the bacterial cell wall has been observed in cultures of *Myxococcus xanthus* during bacterially induced calcification (Rodriguez-Navarro *et al.* 2007). This is one of the very few studies showing such a pattern involving prokaryote cells. In contrast, abundant mesocrystals have been observed in several eukaryote biomineralizing systems such as corals (Cuif & Dauphin 2005; Przeniosło *et al.* 2008; Vielzeuf *et al.* 2008), including oriented aragonite nanocrystals within centers of

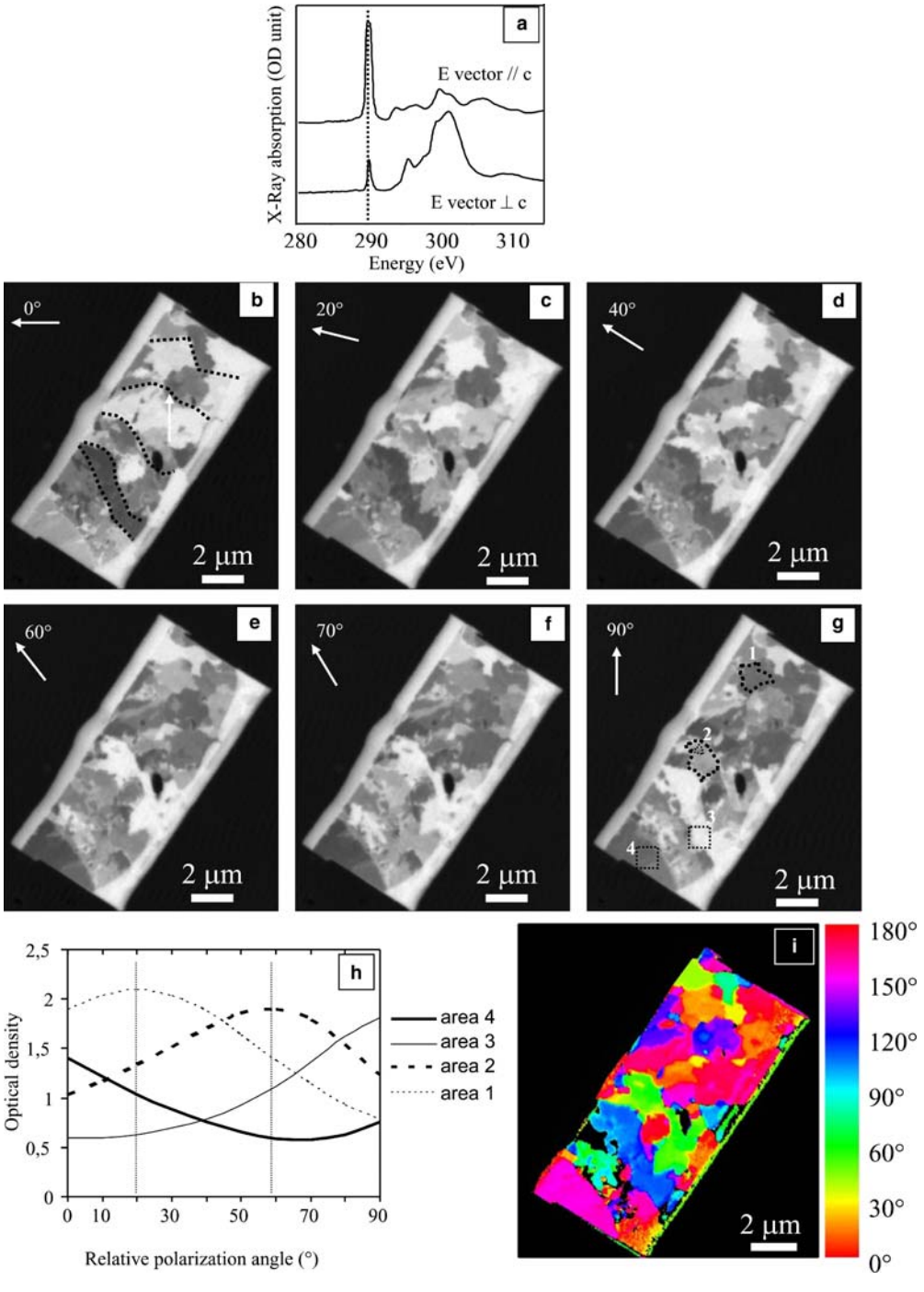

Fig. 6. STXM mapping of the orientation of the *c*-axis of aragonite in the FIB foil. (**a**) XANES spectra at the C K-edge of a single aragonite crystal measured at two perpendicular orientations of the beam polarization, either parallel or perpendicular to the *c*-axis of aragonite. The dashed line indicates the absorption peak at 290.3 eV attributed to 1s $\rightarrow$ π^* electronic transitions of carbonate groups. Absorption at this energy is higher when the polarization vector of the beam is parallel to the *c*-axis of aragonite, and lower when perpendicular. (**b–g**) STXM images taken at 290.3 eV of the FIB foil with varying directions of the polarization of the incident X-ray beam (0, 20, 40, 60, 70 and 90°),

rapid accretion of corals (Benzerara *et al.* in rev.), sponge spicules (Sethmann *et al.* 2006), and mollusc nacre (Rousseau *et al.* 2005) as well as in abiotic systems deprived of organics (e.g. Niederberger & Colfen 2006). Although it has been proposed that the formation of such mesocrystals may involve specific and controlled biological processes, the stromatolite and the abiotic occurrences of aragonite mesocrystals underline the fact that as long as the molecular processes leading to crystallographic alignment of these nanodomains are ignored, little can be concluded about the biospecificity of such objects.

The evolution of the crystallographic orientation of the crystals within aragonite laminae is an additional issue to discuss. Observations of the Satonda stromatolites by transmitted light microscopy suggest that aragonite fibres are globally oriented perpendicular to the laminae. Interestingly, such a structure with well-oriented aragonite crystals is also observed in nacre for example, in which aragonite tablets grow in alternation with organic matrix sheets. Recently, Coppersmith *et al.* (2009) proposed a model to explain how a greater orientational order develops over a distance of several aragonite tablets. The model is based on two assumptions: (1) well-oriented tablets grow faster than misoriented ones; and (2) the crystal orientation of a tablet from a given layer is highly probable to be the same as that of the tablet directly below its nucleation site. This latter assumption reflects the presence of pores in the organic matrix that allow some kind of 'communication' between the successive aragonite tablet layers. In Satonda stromatolites, the Mg–Si-rich layers separate the aragonite layers. However, the map of the orientation of aragonite *c*-axis (Fig. 6) and TEM images do not show any 'transmission' of the crystal orientation through the Mg–Si-rich layer. On the FIB foil observed in the present study, only a few crystals were found to have their *c*-axes oriented perpendicular to the laminae, except aragonite fibres at the top of the underlying laminae. Two issues remain unresolved: (1) how aragonite crystals become eventually oriented within an aragonite laminae? And (2) why aragonite crystals in a given cluster do not influence the orientation of aragonite crystals forming on top? More observations of whole aragonite laminae, also involving additional techniques that provide a larger scale view of the crystallographic orientation of aragonite, will be needed in order to better understand how the general orientation of aragonite crystals eventually evolved towards a preferred crystallographic orientation of the fibres within a single lamina.

Finally, the striations observed within the aragonite laminae and parallel to them remain unexplained. Texturally, they look similar to the growth bands observed in corals (Fig. 2) and hence there could be a general mechanism responsible for their formation in stromatolites and corals. This mechanism would be important to decipher in order to understand whether it is related to variations in the biological activity and/or whether it is associated with some temporal periodicity of the environment. However, we could not detect in the Satonda stromatolites the significant Mg and Sr variations observed in corals. The meaning of such compositional variations is, however, still discussed in the coral literature (e.g. Meibom *et al.* 2004), and further studies detailing the ultrastructural variations responsible for their formation are required to better assess the similarities and differences of these features in corals and stromatolites. One possibility that will require a more systematic investigation is that these rings correspond to the 1–2 μm thick areas evidenced by STXM in which the orientation of the aragonite crystals is roughly the same (Fig. 6). They would correspond to successive episodes of precipitation with variations in the growth direction of aragonite crystals.

In conclusion, the present study provides (1) a new description of Satonda stromatolites at the nm-scale, which is, in our opinion, an important basis for future comparisons; and (2) a new methodological framework offering an unprecedented description down to the nm-scale of the mineralogy and texture of carbonate minerals and that might be of interest to the scientific communities studying stromatolites, speleothems, travertines and tufas. Finally, the present study proposes speculative yet heuristic working hypotheses based on a tentative

Fig. 6. (*Continued*) indicated by arrows. Brighter areas absorb more, darker areas absorb less. For a single pixel, the variation of intensity between the different images is due to linear dichroism. Pixels showing similar variations have a common orientation of the in-plane projection of the *c*-axis of aragonite. Dashed curves in (b) delimit areas in which grains roughly show a consistent crystallographic orientation of the aragonite *c*-axis with significant deviations toward the upper right corner. (**h**) Plot of the variation of absorption with the direction of the polarization vector for different areas chosen in the FIB foil. The curves can be fit as $A\cos^2(\theta - \phi) + B$. The maximum of absorption gives the angular direction of the *c*-axis of aragonite (ϕ). Maximum absorption for areas 1, 2, 3, 4 are at 18°, 54°, 107° and 155°, respectively. (**i**) Map of the orientation of the in-plane projection of the *c*-axis of aragonite in the FIB foil. Areas in black do not contain aragonite and were not fitted. The spatial resolution (i.e. the size of the pixels that were fitted) of this map is 50 nm.

comparison between stromatolites and corals that question the mechanisms of nucleation and growth of carbonates in these structures and the way these structures are or are not controlled at the meso- and macroscale. It is obvious that our observations and the resulting understanding of the texture of carbonates in stromatolites at the submicrometre-scale are still very limited. Additional studies of this type on other samples should offer new insights about the biological and abiotic processes involved in the formation of such structures with significant implications regarding the search for traces of ancient life on Earth.

This work was partly funded by the ANR 'Jeunes Chercheurs' grant NanoGeobio #06-JCJC-0158-02 (Anders Meibom and Karim Benzerara). This work was also supported in part by NSF Grant CHE-0431425 (Stanford Environmental Molecular Science Institute).The microbialites were sampled during German-Indonesian Expedition to Satonda Lake 1993 (led by Stephan Kempe, Darmstadt) supported by the Deutsche Forschungsgemeinschaft. JS was funded by the Polish Ministry of Science and Higher Education, project N307-015733. The National NanoSIMS facility at the Muséum National d'Histoire Naturelle was established by funds from the CNRS, Région Île de France, Ministère délégué à l'Enseignement supérieur et à la Recherche, and the Muséum itself. We thank Omar Boudouma from the Laboratory Magie at University Pierre et Marie Curie (Paris, France) who performed the SEM analyses on the Zeiss Supra 55 SEM microscope. Finally, we thank Emmanuelle Porcher (UMR 7254, MNHN Paris, France) for programming the R routine fitting the STXM polarization-dependent data.

References

ALLWOOD, A. C., WALTER, M. R., KAMBER, B. S., MARSHALL, C. P. & BURCH, I. W. 2006. Stromatolite reef from the Early Archaean era of Australia. *Nature*, **441**, 714–718.

ALOISI, G., GLOTER, A., KROGER, M., WALLMANN, K., GUYOT, F. & ZUDDAS, P. 2006. Nucleation of calcium carbonate on bacterial nanoglobules. *Geology*, **34**, 1017–1020.

ALTERMANN, W., KAŹMIERCZAK, J., OREN, A. & WRIGHT, D. T. 2006. Cyanobacterial calcification and its rock-building potential during 3.5 billion years of Earth history. *Geobiology*, **4**, 147–166.

ARP, G., REIMER, A. & REITNER, J. 2003. Microbialite formation in seawater of increased alkalinity, Satonda crater lake, Indonesia. *Journal of Sedimentary Research*, **73**, 105–127.

BENZERARA, K., MENGUY, N., GUYOT, F., VANNI, C. & GILLET, P. 2005. TEM study of a silicate-carbonate-microbe interface prepared by focused ion beam milling. *Geochimica et Cosmochimica Acta*, **69**, 1413–1422.

BENZERARA, K., MENGUY, N., LOPEZ-GARCIA, P., YOON, T. H., KAŹMIERCZAK, J., TYLISZCZAK, T., GUYOT, F. & BROWN, G. E. JR. 2006. Nanoscale detection of organic signatures in carbonate microbialites. *Proceedings of the National Academy of Sciences of the United States of America*, **103**, 9440–9445.

BENZERARA, K., MORIN, G., YOON, T. H., MIOT, J., TYLISZCZAK, T., CASIOT, C., BRUNEEL, O., FARGES, F. & BROWN, G. E. JR. 2008. Nanoscale study of As biomineralization in an acid mine drainage system. *Geochimica et Cosmochimica Acta*, **72**, 3949–3963.

BENZERARA, K., MENGUY, N., OBST, M., STOLARSKI, J., MAZUR, M., TYLISCZAK, T., BROWN, G. E. JR. & MEIBOM, A. Nanoscale skeletal architecture of a scleractinian coral. Submitted to *Proceedings of the Royal Society B*.

BERNARD, S., BENZERARA, K., BEYSSAC, O., MENGUY, N., GUYOT, F., BROWN, G. E. JR. & GOFFE, B. 2007. Exceptional preservation of fossil plant spores in high-pressure metamorphic rocks. *Earth and Planetary Science Letters*, **262**, 257–272.

BLUHM, H. K., ANDERSSON, T. *ET AL.* 2006. Soft X-ray microscopy and spectroscopy at the molecular environmental science beamline at the Advanced Light Source. *Journal of Electron Spectroscopy and Related Phenomena*, **150**, 86–104.

BRAISSANT, O., CAILLEAU, G., DUPRAZ, C. & VERRECCHIA, E. P. 2003. Bacterially induced mineralization of calcium carbonate in terrestrial environments: the role of exopolysaccharides and amino acids. *Journal of Sedimentary Research*, **73**, 485–490.

BRAISSANT, O., DECHO, A. W., DUPRAZ, C., GLUNK, C., PRZEKOP, K. M. & VISSCHER, P. T. 2007. Exopolymeric substances of sulfate-reducing bacteria: Interactions with calcium at alkaline pH and implication for formation of carbonate minerals. *Geobiology*, **5**, 401–411.

COPPERSMITH, S. N., GILBERT, P. U. P. A. & METZLER, R. A. 2009. Theoretical characterization of a model of aragonite crystal orientation in red abalone nacre. *Journal of Physics A – Mathematical and Theoretical*, **42**, Article Number: 125101.

CUIF, J. P. & DAUPHIN, Y. 2005. The two-step mode of growth in the Scleractinian coral skeletons from the micrometre to the overall scale. *Journal of Structural Biology*, **150**, 319–331.

DUPRAZ, C. & VISSCHER, P. T. 2005. Microbial lithification in marine stromatolites and hypersaline mats. *Trends in Microbiology*, **13**, 429–438.

DUPRAZ, C., VISSCHER, P. T., BAUMGARTNER, L. K. & REID, R. P. 2004. Microbe–mineral interactions: early carbonate precipitation in a hypersaline lake (Eleuthera Island, Bahamas). *Sedimentology*, **51**, 745–765.

DUPRAZ, C., PATTISINA, R. & VERRECCHIA, E. P. 2006. Translation of energy into morphology: simulation of stromatolite morphospace using a stochastic model. *Sedimentary Geology*, **185**, 185–203.

GIBBS, W. W. & POWELL, C. S. 1996. Bugs in the data? The controversy over Martian life is just beginning. *Scientific American*, **275**, 20.

GROTZINGER, J. P. & ROTHMAN, D. H. 1996. An abiotic model for stromatolite morphogenesis. *Nature*, **383**, 423–425.

HABERSTROH, P. R., BRANDES, J. A., GELINAS, Y., DICKENS, A. F., WIRICK, S. & CODY, G. 2006.

Chemical composition of the graphitic black carbon fraction in riverine and marine sediments at submicron scales using carbon X-ray spectromicroscopy. *Geochimica et Cosmochimica Acta*, **70**, 1483–1494.

HEANEY, P. J., VICENZI, E. P., GIANNUZZI, L. A. & LIVI, K. L. T. 2001. Focused ion beam milling: a method of site-specific sample extraction for microanalysis of Earth and planetary materials. *American Mineralogist*, **86**, 1094–1099.

HITCHCOCK, A. P. 2001. Soft X-ray spectromicroscopy of polymers and biopolymer interfaces. *Journal of Synchrotron Radiation*, **8**, 66–71.

HOFMANN, H. J. 2000. Archean stromatolites as microbial archives. *In*: RIDING, R. & AWRAMIK, S. M. (eds) *Microbial Sediments*. Springer-Verlag, Berlin, Heidelberg, 315–327.

KAWAGUCHI, T. & DECHO, A. W. 2002. *In situ* microspatial imaging using two-photon and confocal laser scanning microscopy of bacteria and extracellular polymeric secretions (EPS) within marine stromatolites. *Marine Biotechnology*, **4**, 127–131.

KAŹMIERCZAK, J. & KEMPE, S. 2004. Microbialite formation in seawater of increased alkalinity, Satonda Crater Lake, Indonesia – Discussion. *Journal of Sedimentary Research*, **74**, 314–317.

KAŹMIERCZAK, J., KEMPE, S. & ALTERMANN, W. 2004. Microbial origin of Precambrian carbonates: lessons from modern analogues. *In*: ERIKSSON, P. G., ALTERMANN, W., NELSON, D. R., MUELLER, W. U. & CATUNEANU, O. (eds) *The Precambrian Earth: Tempos and Events*. Elsevier, Amsterdam, 545–564.

KEMPE, S. & KAŹMIERCZAK, J. 1993. Satonda Crater Lake, Indonesia: Hydrogeochemistry and Biocarbonates. *Facies*, **28**, 1–31.

KEMPE, S. & KAŹMIERCZAK, J. 2007. Hydrochemical key to the genesis of calcareous non-laminated and laminated cyanobacterial microbialites. *In*: SECKBACH, J. (ed.) *Algae and Cyanobacteria in Extreme Environments*. Springer, Dordrecht, 239–264.

KREMER, B., KAŹMIERCZAK, J. & STAL, L. J. 2008. Calcium carbonate precipitation in cyanobacterial mats from sandy tidal flats of the North Sea. *Geobiology*, **6**, 46–56.

KÜHL, M., FENCHEL, T. & KAZMIERCZAK, J. 2003. Structure, function, and calcification potential of an artificial cyanobacterial mat. *In*: KRUMBEIN, W. E., PATERSON, D. & ZAVARZIN, G. (eds) *Fossil and Recent Biofilms – A Natural History of Life on Earth*. Kluver Academic Publishers, Dordrecht, 77–102.

LEPOT, K., BENZERARA, K., BROWN, G. E. JR. & PHILIPPOT, P. 2008. Microbially influenced formation of 2,724-million-year-old stromatolites. *Nature Geoscience*, **1**, 118–121.

LOWE, D. R. 1994. Abiological origin of described stromatolites older than 3.2 Ga. *Geology*, **22**, 387–390.

MCLOUGHLIN, N., WILSON, L. A. & BRASIER, M. D. 2008. Growth of synthetic stromatolites and wrinkle structures in the absence of microbes – implications for the early fossil record. *Geobiology*, **6**, 95–105.

MEIBOM, A., CUIF, J. P., HILLION, F. O., CONSTANTZ, B. R., JUILLET-LECLERC, A., DAUPHIN, Y., WATANABE, T. & DUNBAR, R. B. 2004. Distribution of magnesium in coral skeleton. *Geophysical Research Letters*, **31**.

MEIBOM, A., MOSTEFAOUI, S., CUIF, J. P., DAUPHIN, Y., HOULBREQUE, F., DUNBAR, R. B. & CONSTANTZ, B. R. 2007. Biological forcing controls the chemistry of reef-building coral skeleton. *Geophysical Research Letters*, **34**, #L02601.

MEIBOM, A., CUIF, J. P., HOULBREQUE, F., OSTEFAOUI, S., DAUPHIN, Y., MEIBOM, K. L. & DUNBAR, R. B. 2008. Compositional variations at ultra-structure length scales in coral skeleton. *Geochimica et Cosmochimica Acta*, **72**, 1555–1569.

METZLER, R. A. D., ZHOU, M. *ET AL*. 2008. Polarization-dependent imaging contrast in abalone shells. *Physical Review B*, **77**, #064110.

NIEDERBERGER, M. & COLFEN, H. 2006. Oriented attachment and mesocrystals: Non-classical crystallization mechanisms based on nanoparticle assembly. *Physical Chemistry Chemical Physics*, **8**, 3271–3287.

PERRIN, C. & SMITH, D. C. 2007. Earliest steps of diagenesis in living scleractinian corals: Evidence from ultrastructural pattern and Raman spectroscopy. *Journal of Sedimentary Research*, **77**, 495–507.

PETRISOR, A. I., KAWAGUCHI, T. & DECHO, A. W. 2004. Quantifying $CaCO_3$ microprecipitates within developing surface mats of marine stromatolites using GIS and digital image analysis. *Geomicrobiology Journal*, **21**, 491–496.

PRZENIOSŁO, R., STOLARSKI, J., MAZUR, M. & BRUNELLI, M. 2008. Hierarchically structured scleractinian coral biocrystals. *Journal of Structural Biology*, **161**, 74–82.

REID, R. P. P. T., VISSCHER, A. W. *ET AL*. 2000. The role of microbes in accretion, lamination and early lithification of modern marine stromatolites. *Nature*, **406**, 989–992.

RIDING, R. 2000. Microbial carbonates: the geological record of calcified bacterial–algal mats and biofilms. *Sedimentology*, **47**, 179–214.

RODRIGUEZ-NAVARRO, C., JIMENEZ-LOPEZ, C., RODRIGUEZ-NAVARRO, A., GONZALEZ-MUNOZ, M. T. & RODRIGUEZ-GALLEGO, M. 2007. Bacterially mediated mineralization of vaterite. *Geochimica et Cosmochimica Acta*, **71**, 1197–1213.

ROUSSEAU, M., LOPEZ, E., STEMPFLE, P., BRENDLE, M., FRANKE, L., GUETTE, A., NASLAIN, R. & BOURRAT, X. 2005. Multiscale structure of sheet nacre. *Biomaterials*, **26**, 6254–6262.

SCHOPF, J. W., KUDRYAVTSEV, A. B., CZAJA, A. D. & TRIPATHI, A. B. 2007. Evidence of archean life: stromatolites and microfossils. *Precambrian Research*, **158**, 141–155.

SEMIKHATOV, M. A., GEBELEIN, C. D., CLOUD, P., AWRAMIK, S. M. & BENMORE, W. C. 1979. Stromatolite morphogenesis – progress and problems. *Canadian Journal of Earth Sciences*, **16**, 992–1015.

SETHMANN, I., PUTNIS, A., GRASSMANN, O. & LOBMANN, P. 2005. Observation of nano-clustered calcite growth via a transient phase mediated by organic polyanions: a close match for biomineralization. *American Mineralogist*, **90**, 1213–1217.

SETHMANN, I., HINRICHS, R., WORHEIDE, G. & PUTNIS, A. 2006. Nano-cluster composite structure of calcitic sponge spicules – a case study of basic characteristics

of biominerals. *Journal of Inorganic Biochemistry*, **100**, 88–96.

SHAPIRO, R. S. 2000. A comment on the systematic confusion of thrombolites. *Palaios*, **15**, 166–169.

STEELE, A., GODDARD, D., BEECH, I. B., TAPPER, R. C., STAPLETON, D. & SMITH, J. R. 1998. Atomic force microscopy imaging of fragments from the Martian meteorite ALH84001. *Journal of Microscopy, Oxford*, **189**, 2–7.

STOLARSKI, J. 2003. Three-dimensional micro- and nanostructural characteristics of the scleractinian coral skeleton: A biocalcification proxy. *Acta Palaeontologica Polonica*, **48**, 497–530.

TODD, P. A. 2008. Morphological plasticity in scleractinian corals. *Biological Reviews*, **83**, 315–337.

VIELZEUF, D., GARRABOU, J., BARONNET, A., GRAUBY, O. & MARSCHAL, C. 2008. Nano to macroscale biomineral architecture of red coral (*Corallium rubrum*). *American Mineralogist*, **93**, 1799–1815.

VISSCHER, P. T., REID, R. P. & BEBOUT, B. M. 2000. Microscale observations of sulfate reduction: Correlation of microbial activity with lithified micritic laminae in modern marine stromatolites. *Geology*, **28**, 919–922.

ZHOU, D., METZLER, R. A., TYLISZCZAK, T., GUO, J. H., ABRECHT, M., COPPERSMITH, S. N. & GILBERT, P. 2008. Assignment of Polarization-Dependent Peaks in Carbon K-Edge Spectra from Biogenic and Geologic Aragonite. *Journal of Physical Chemistry B*, **112**, 13 128–13 135.